WAVE INTERACTION WITH BERM BREAKWATERS

By Marcel R. A. Van Gent[1]

ABSTRACT: Wave interaction with berm breakwaters is studied by means of a physical model and a numerical model. The physical-model tests have been used to verify the wave motion as calculated by the numerical model. The numerical model based on finite-amplitude shallow-water wave equations is capable of simulating the wave motion both on and inside the structure. This model for normally incident waves has been extended with a new morphological model for cross-structure transport, which resulted in a wave load-response model capable of simulating the reshaping process of the seaward slopes of dynamic coastal structures such as berm breakwaters and gravel beaches. The combined wave-morphological model has been verified with small-scale laboratory tests and with prototype data. Trends observed in physical model tests, such as the influence of wave height, wave period, and stone diameter on the reshaped seaward slopes, are also reproduced properly.

INTRODUCTION

Berm breakwaters are a relatively new type of structure. Their natural response to hydrodynamic loads makes them economically attractive, not in the least because smaller rock material can be used than with conventional breakwaters. On the other hand, the dynamic behavior, typical of berm breakwaters requires special attention. The seaward slope undergoes reshaping until a stable seaward profile has developed. This dynamic behavior of the seaward slope is very dependent on the hydrodynamic loads and vice versa. This interactive character of the hydrodynamics and the reshaping process are studied here.

In Van Gent (1994a) a numerical model for simulating wave motion on a structure and inside a permeable structure is described. The wave dynamics of a normally incident wave attack on various types of structures are approximated by the nonlinear shallow-water equations with steep wave fronts represented by bores. For this one-dimensional description of the wave motion, the vorticity and vertical accelerations are assumed to be negligibly small, which leads to hydrostatic pressure. Depth-averaged velocities are used, and only one free surface point per cross section is defined. This, however, leads to incapability of simulating the overturning wave tongue of plunging breakers.

Based on the nonlinear shallow-water equations, Hibberd and Peregrine (1979) developed a numerical model with an explicit dissipative finite-difference scheme (Lax-Wendroff). Using this concept, many practical applications have been obtained [see, for instance, Kobayashi et al. (1987)] for wave reflection and runup on impermeable rough slopes. For the permeable part of a structure, the same types of equations can be applied although the friction coefficients for the porous medium need to be assessed; see Van Gent (1994b). A proper coupling of the external flow to the internal flow is applied in Van Gent (1994a). After several validations, applications, and extensions, the model has now become a user-friendly personal-computer model for practice-based and research-based engineers. The model is able to deal with either regular or irregular waves, which attack various types of structures with arbitrary seaward slopes, smooth or rough, permeable or impermeable, overtopped or not. In addition, the program accounts for several phenomena such as reflection, transmission, overtopping, infiltration, seepage, varying roughness along the slope, linear and nonlinear porous friction, added mass, and the disconnection of the free surface and the phreatic surface. Besides the wave conditions of the incident waves (wave height, wave period, or a specific incident wave train), the still-water level, the slopes of the cover layer and of the core, the stone diameter, and the porosity need to be prescribed to run the model. The friction along the slope can be varied, although recommended values are given in which the stone diameter determines the friction coefficient. Although the model is one-dimensional, it can give a useful impression of the flow field in two dimensions (see Figs. 1 and 2).

An additional verification of the preceding numerical model has been performed by studying the wave motion above the seaward slope of a small-scale model of a berm breakwater. The physical-model tests will be discussed before describing the extension of the numerical model with a morphological cross-structure model.

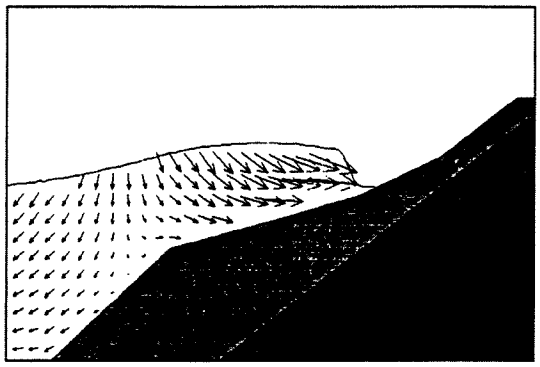

FIG. 1. Impression of Flow Field on and in Berm Breakwater with Impermeable Core

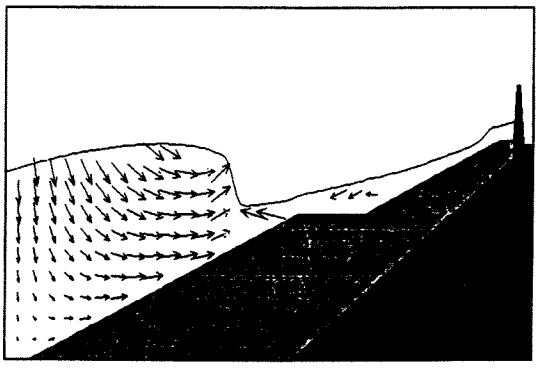

FIG. 2. Impression of Flow Field on and in Permeable Structure with a Crown Wall

[1]Res. Engr., Delft Hydraulics, P.O. Box 152, 8300 AD Emmelord, The Netherlands.

Note. Discussion open until March 1, 1996. To extend the closing date one month, a written request must be filed with the ASCE Manager of Journals. The manuscript for this paper was submitted for review and possible publication on May 16, 1994. This paper is part of the ***Journal of Waterway, Port, Coastal, and Ocean Engineering***, Vol. 121, No. 5, September/October, 1995. ©ASCE, ISSN 0733-950X/95/0005-0229–0238/ $2.00 + $.25 per page. Paper No. 8434.

PHYSICAL MODEL

Physical-model tests have been performed to verify numerical model results. The flow field has been recorded using video, electromagnetic flow meters, wave-height meters, and pressure transducers. Fig. 3 shows a cross section of the experimental setup with the berm breakwater model and the positions of the eight pressure transducers inside the berm.

The test results have been used for both qualitative and quantitative verification of the one-dimensional model as discussed in the previous section and for a two-dimensional model, discussed in Van Gent et al. (1995). Here, a discussion of the test results and a comparison with results from the 1-D model, described in detailed in Van Gent (1993), will be given.

Fig. 4 shows the profile development of the seaward profile after four series of 1,000 regular waves. After each wave series, waves with a new combination of wave height and wave period, resulting in a larger impact on the slope, were imposed without restoring the seaward profile. After the seaward profile had reached its final reshaped profile, eight series of regular waves were imposed on this last reshaped profile. From the analysis of these wave series, detailed information on the flow field was obtained, both inside and outside the structure.

The analysis of the video images resulted in figures where the surface elevations are shown in the area above the berm of the structure at certain moments of time. Fig. 5 shows an example of such a snapshot. The area in between the two

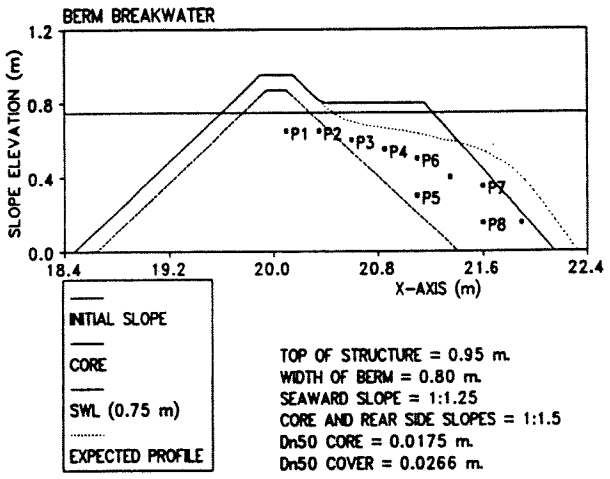

FIG. 3. Cross Section of Berm Breakwater in Experimental Setup with Pressure Transducers

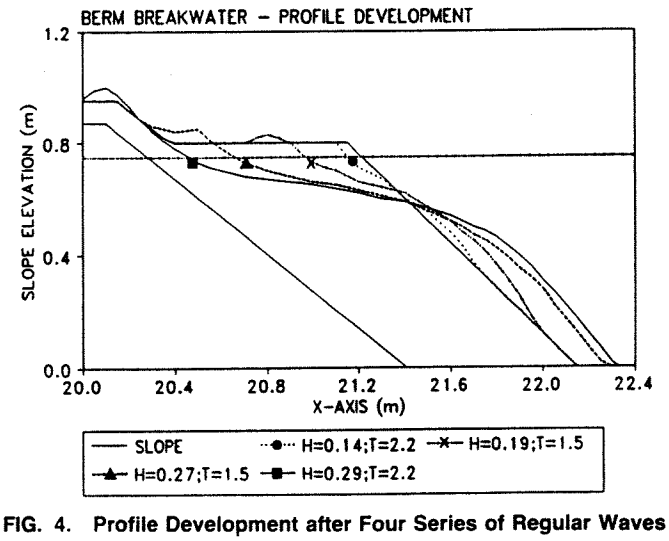

FIG. 4. Profile Development after Four Series of Regular Waves

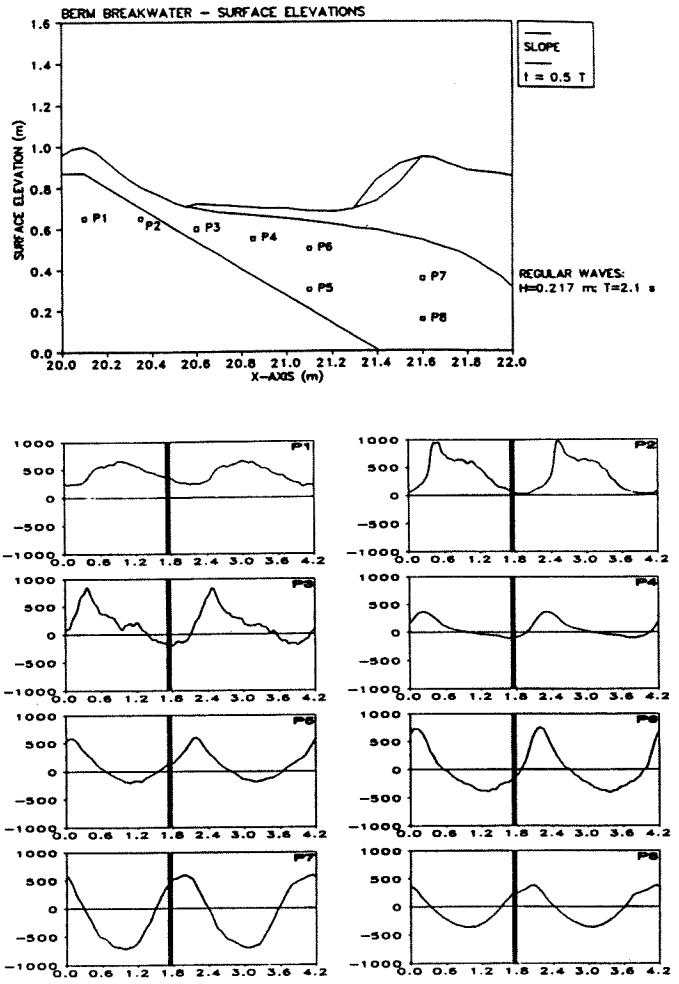

FIG. 5. Measured Surface Elevation and Corresponding Pressure (Pa) from Eight Transducers as Function of Time (s)

lines in this figure indicates the region where air is enclosed. The moments of time corresponding to this snapshot are indicated by solid vertical lines in the signals from the pressure transducers shown in the lower part of this figure. The zero pressures correspond to the pressure during still water. The positions of the pressure transducers are indicated in the snapshot printed in the upper part of Fig. 5.

The signals from the pressure transducers show that the pressures inside the berm do follow the fluctuations of the free surface in the same cross section quickly; the maxima of the measured pore pressures occur at nearly the same moments of time at which the free surface above the transducers have maxima.

The pressure fluctuations in two cross sections have been analyzed. In each cross section, two pressure transducers were positioned at $x = 21.1$ m (P5 and P6) and at $x = 21.6$ m (P7 and P8) (see Fig. 3). The maximum positive pressures minus the minimum pressures are shown in Figs. 6 and 7; they show pressure fluctuations depending on the vertical position. The fluctuations of the free surface are incorporated by using the maximum minus the minimum free surface elevation at that cross section. In Figs. 6 and 7, these fluctuations are printed at the average water level. The figures show that the fluctuations of the free surface do not fully penetrate into the permeable part.

VERIFICATION OF HYDRODYNAMICS

Measurements with eight series of regular waves have been analyzed and compared with numerical model results. In the

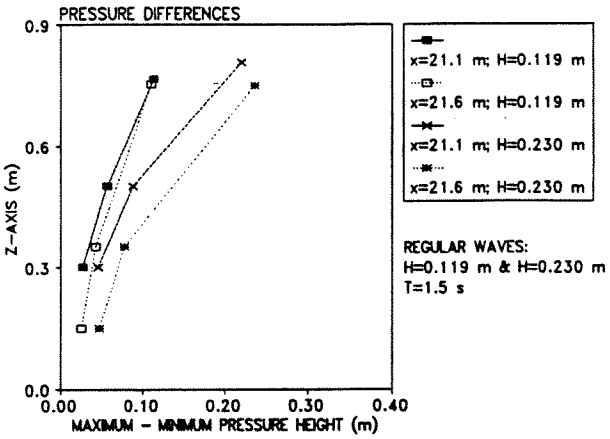

FIG. 6. Pressure Fluctuations as Function of Vertical Position, T = 1.5 s

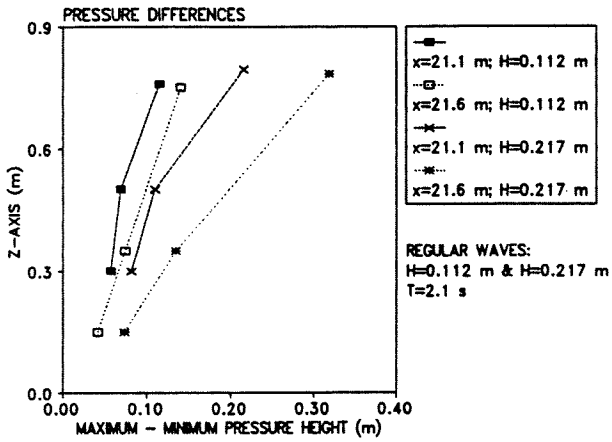

FIG. 7. Pressure Fluctuations as Function of Vertical Position, T = 2.1 s

computations, the reshaped seaward slope of the berm breakwater was represented by five straight sections. The crest level was 1.00 m. In the numerical model, the structure was modeled as a homogeneous structure with a porosity of 0.417 (measured in situ) and a stone diameter (D_{n50} of 0.0266 m. This means that the permeable core (n = 0.418, D_{n50} = 0.0175 m) is represented by the same material as the cover layers. For the friction coefficient f, 0.10 has been used in all simulations. For the still-water level, the average water level in the section between the wave generator and the structure has been used.

Figs. 8(a)–(d) show some comparisons between measured surface elevations assessed by analysis of the video pictures as well as numerical results from the 1-D model. Waves with the combinations of wave height and wave period of H = 0.119 m and T = 1.5 s, H = 0.230 m and T = 1.5 s, and H = 0.217 m and T = 2.1 s are shown. For each wave series, two figures with measured surface elevations are given [Figs. 8(a) and 8(c)]. The first figure for each wave condition shows five moments of time within the first half of the wave cycle. The second figure shows five moments of time within the second half of the wave cycle. Figs. 8(b) and 8(d) show the computed surface elevations at the same moments of time as the measured elevations given in Figs. 8(a) and 8(c).

The comparison between measured and computed surface elevations show that the numerical results give a rather good impression of the wave action until the position where air is captured (first half of the wave cycle). Because entrapped air cannot be modeled with the 1-D model, behind this point with entrapped air the resemblance in the second half is much

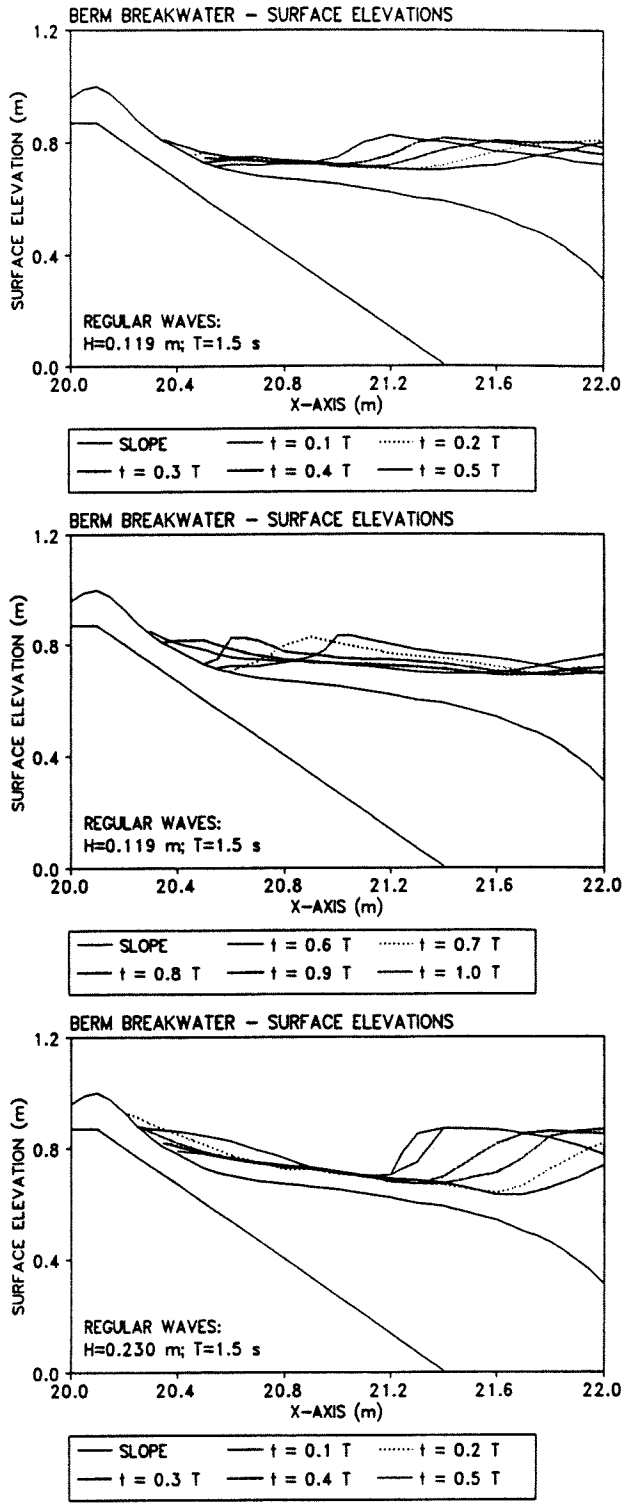

FIG. 8a. Measured Surface Elevations

weaker. The calculated waves evolve somewhat quicker than in reality. This is due to the approximation by the nonlinear shallow-water equations.

Fig. 9 shows both the measured and calculated values for runup and rundown levels. The runup values are represented rather well. For the rundown levels, the computations with wave periods of 1.5 s were rather accurate. The computations with a wave period of 2.1 s do show the correct trend but absolute differences of 0.04 m occur. Computations with an impermeable structure also indicated that the runup levels were represented rather accurately (Van Gent 1994a). This was not the case for the rundown levels. The same conclusions

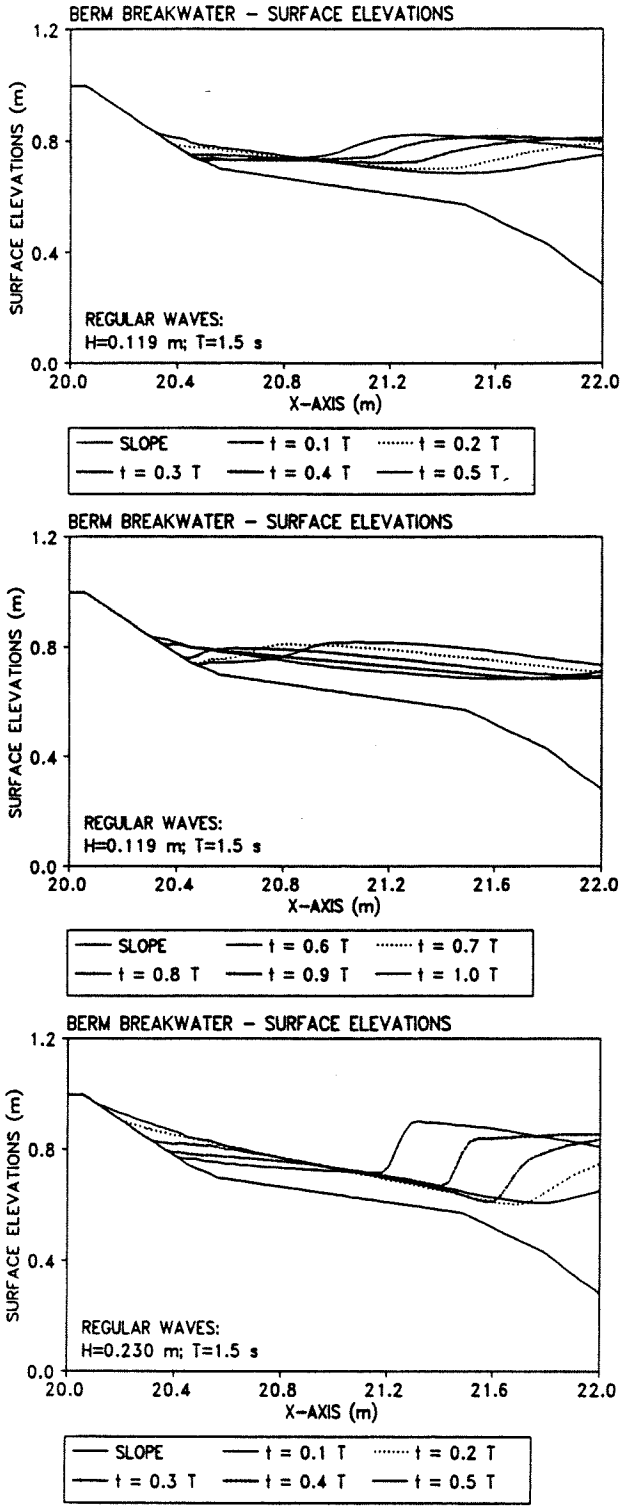

FIG. 8b. Calculated Surface Elevations for Comparison with Measured Elevations in Fig. 8(a)

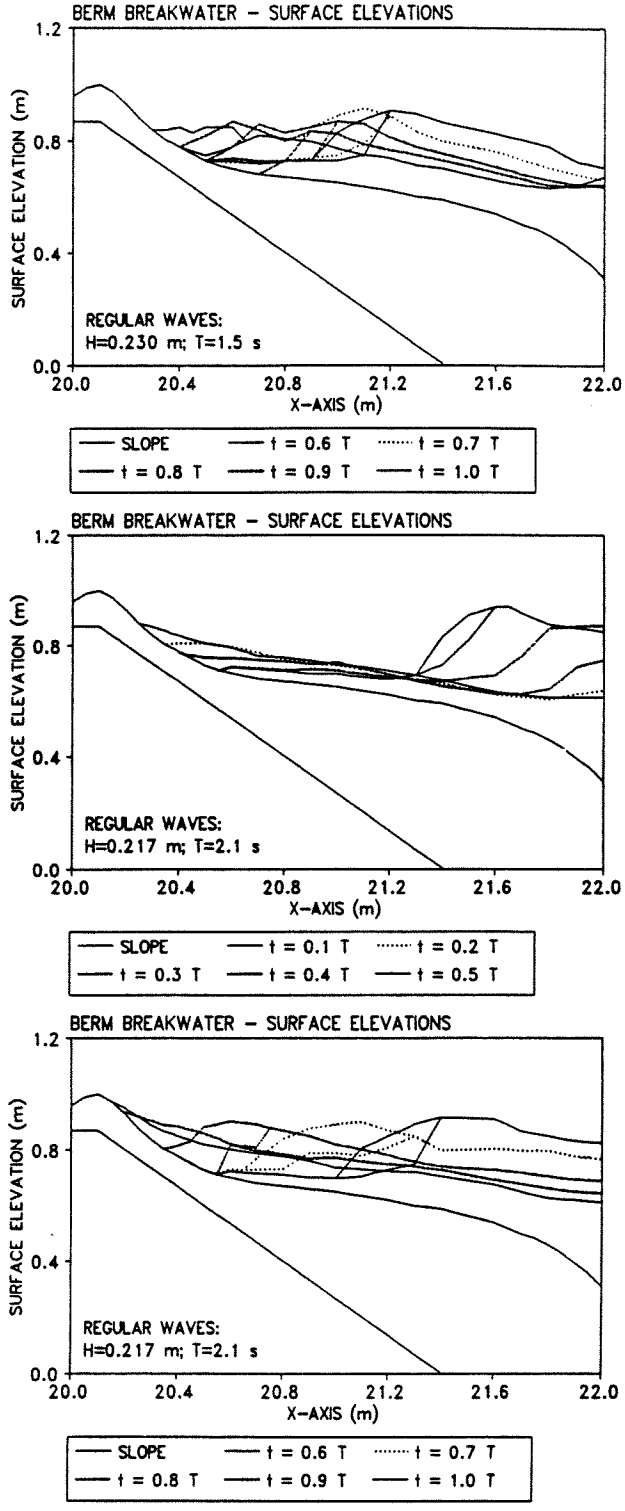

FIG. 8c. Measured Surface Elevations

can be drawn here. The runup and rundown levels were measured visually and checked using the video images. Because during runup the thickness of the water layers were smaller than the dimensions of the stones, differences between the observed and actual runup levels may have occurred (differences estimated at less than 0.01 m).

From the comparison with physical-model results, it can be concluded that the numerical results give a satisfactory impression of the wave motion for normally incident waves on berm breakwaters. Therefore, the numerical model has been extended with a module for the morphological development of the seaward slope of dynamically stable structures such as berm breakwaters and gravel beaches. The module is based on simulations of individual displacements of stones. For this process a new approach has been developed, which is described in the following section.

RESPONSE MODEL

For rubble-mound and berm breakwaters, the stability of individual stones in the seaward slope and the stability of the seaward slope itself are among the most important aspects for the functionality of a breakwater.

The stability of the stones is strongly dependent on the hydrodynamic properties. Several expressions for this stabil-

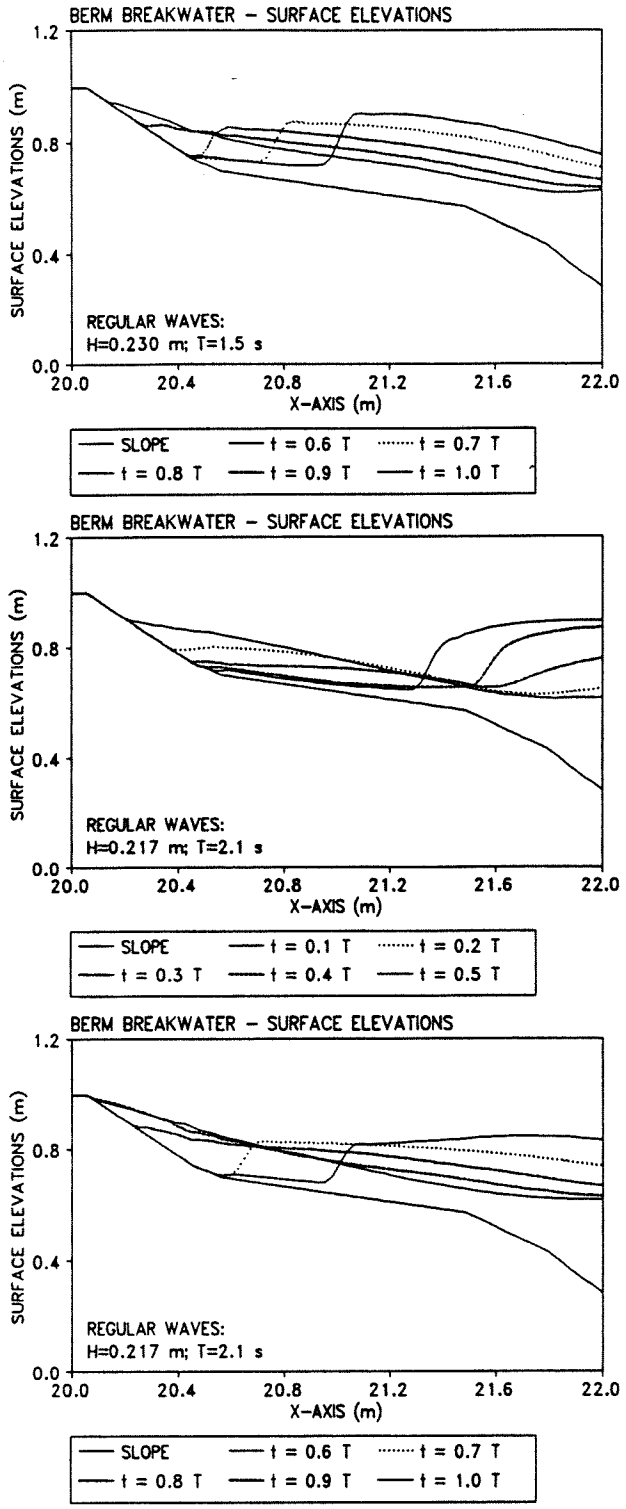

FIG. 8d. Calculated Surface Elevations for Comparison with Measured Elevations in Fig. 8(c)

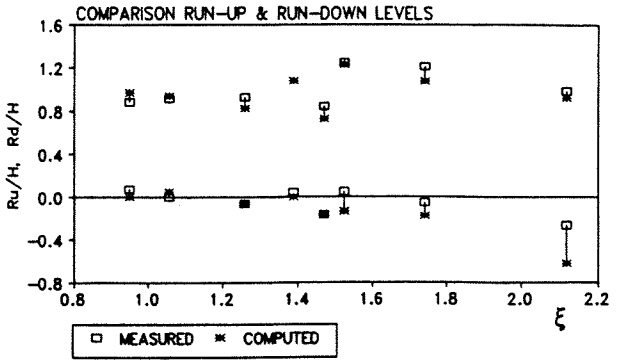

FIG. 9. Comparison between Measured and Calculated Runup and Rundown Levels

ity have been developed. Iribarren Cavanilles (1938) and Hudson (1958) derived widely used expressions where the hydrodynamic properties are represented by the wave height. Van der Meer (1988) performed many laboratory tests to study the influence of other hydrodynamic properties as well. The results were summarized in empirical relations that also contain hydraulic parameters such as wave period and the number of waves. The relations are valid for a wide range of parameters. However, it can be useful to study the reshaping process in a more detailed way. This can be done to model the reshaping process numerically by using hydrodynamic properties such as velocities and accelerations. Such a numerical approach can be used to exclude possible influences of scale effects and study the influence of permeability of structures in a more detailed way. The approach can also be used as a complementary design tool. This same procedure could be adapted to model the reshaping process for structures or beaches that contain large immovable components, once the physical processes are better understood. Examples include gravel beaches fronting seawalls and rubble-mound slopes in front of rigid crest elements.

1. The hydrodynamic properties, both outside and inside the structure, need to be known and preferably modeled numerically. The numerical model applied in the previous section can be used as a first approximation for the wave motion.
2. Information concerning the magnitude of forces on stones is necessary. Attempts to measure forces on idealized stones have been performed by Sigurdsson (1962) and Sandstrøm (1974). Tørum (1992) measured forces on a single stone in the cover layer of a berm breakwater.
3. Relations between the forces on stones and the hydrodynamic properties are necessary. As mentioned before, the hydrodynamics can be represented by local velocities and local accelerations. As a first approximation, a Morison-type of expression (Morison et al. 1950) can be used; see, for instance, Tørum (1992) or Kobayashi and Otta (1987).
4. Information concerning failure mechanisms and damage causing forces is needed. Often mechanisms referred to as "rolling," "sliding," or "lifting" are distinguished (e.g. Den Breeker and Vries 1985). These mechanisms or other failure mechanisms need to be modeled.
5. The new positions of the unstable stones need to be known in case one wants to simulate the complete reshaping process. This relocation process needs to be modeled as well. For most breakwaters no severe damage is allowed, so for those cases it is not of primary interest to study the new positions of the stones. However, for berm breakwaters and gravel beaches these new positions are of primary concern.

Norton and Holmes (1992) described a simulation model for the reshaping process of berm breakwaters under normally incident, monochromatic wave attack. Here, a new approach is presented although it is based, as in Norton and Holmes (1992), on individual displacements of stones. As in their approach, this process also bases the initiation of movement of individual stones on a Morison-type of equation including drag, inertia, and lift forces. However, in contrast to the Norton and Holmes approach, the new model can also be applied using irregular waves since its is time-dependent. Fur-

thermore, in the described model, the new positions of unstable stones are determined by the hydrodynamics.

Three forces resulting from the hydrodynamic loads have been identified: drag force (F_D) acting parallel to the slope in the direction of the velocity, the inertia force (F_I) acting parallel to the slope, and the lift force (F_L) acting perpendicularly to the slope. For the drag force and the inertia force, expressions similar as those in the Morison equation can be used. The lift force is the most difficult one to determine. Often the assumption is used that the lift force is proportional to the squared velocity and the squared diameter of the stone. The submerged weight (W_s) has been taken as the countering force.

Because a stone on the surface layer is partially sheltered by other stones, the actual projected area is smaller than for a single stone in a flow. With the area shape factor k_2 this can be incorporated but this has not been done here (Van Gent (1993). The forces have been modeled using the following expressions:

$$F_D = 0.5\rho_w c_D k_2 D^2 u|u| \tag{1}$$

$$F_I = \rho_w c_M k_1 D^3 \frac{Du}{Dt} \tag{2}$$

$$F_L = 0.5\rho_w c_L k_2 D^2 u^2 \tag{3}$$

$$W_s = (\rho_s - \rho_w) g k_1 D^3 \tag{4}$$

where ρ_w = the density of water; ρ_s = the density of the stone material; D = the stone diameter, with D_{EQ} in the numerical model; u = the depth-averaged velocity; c_D = the drag coefficient; c_M = the inertia coefficient; c_L = the lift coefficient; k_1 = the volume shape factor ($\pi/6$ for spheres); k_2 = the area shape factor ($\pi/4$ for spheres); and Du/Dt is approximated by $\partial u/\partial t$.

Several concepts can be used for initiation of movement. The stability condition for the phenomena of lifting and sliding can be expressed by

$$F_L \leq W_s \cos \phi \tag{5}$$

$$|F_D + F_I - W_s \sin \phi| \leq \tan \mu (W_s \cos \phi - F_L) \tag{6}$$

where μ = the angle of internal friction; and ϕ = the local slope angle.

An additional force is implemented at the wave front. The first stone near the wave front is assumed not to be submerged ($W = \rho_s g k_1 D^3$). In the case of velocities in the direction of the stone, the pressure at the wet side of the stone is expressed by the pressure thrust $0.5\rho_w g h^2 D + \rho_w u^2 h D$. In case this force, acting parallel to the slope, exceeds the counteracting component of the weight of the stone, the stone becomes unstable.

The possible direction of unstable moving stones should be assessed. The flow pattern around covering stones is extremely complex. Therefore, the forces as a result of the pressure gradients near the stones are not easy to determine. In the case where the stone is moved out of its position and moves along the slope, the force resulting from a pressure gradient directly depending on the slope of the free surface is assumed to be of importance. This force is assumed to act parallel to the slope; it acts on the volume of the stone and is assumed to be proportional to the gradient of the free surface.

$$F_P = \rho_w c_P g k_1 D^3 \frac{\partial \eta}{\partial x} \tag{7}$$

where η = the free-surface elevation; and c_P = a nondimensional coefficient.

This force as well as the drag, the inertia force and the weight of the stone determine in which direction unstable stones will move. Although for a moving stone the coefficients c_D and c_M are not necessarily the same as those for a stone in the cover layer, this is assumed here at first.

$$(F_D + F_I - F_P - W_s \sin \phi) > 0 \rightarrow \text{upward} \tag{8}$$

$$(F_D + F_I - F_P - W_s \sin \phi) < 0 \rightarrow \text{downward} \tag{9}$$

After determination of the direction in which an unstable stone may move, the local hydrodynamic properties at a position one space increment (Δx) away from the original position will be considered. It is verified whether the stone would be stable or unstable in that neighboring position. If the stone is stable in that position, the stone will stay in its original position. If the stone is also unstable in the neighboring position, the stone will be moved to this new position. This is done without any time delay, which means that the time increment necessary to move the stone one space increment is neglected.

This morphological model for cross-structure transport is interactive with the hydraulic model. At each time step (Δt) the hydraulic properties are determined in all positions. In each position and after each time step, it is verified whether the stones are stable in their present position and whether they need to be relocated. The profile changes due to the movement of the stone. The new profile is immediately incorporated in the hydraulic model.

Some numerical problems remain. If the space increment Δx is equal to the dimension of the stones, a replaced stone can be represented by adjusting the profile with space increment Δz in the vertical direction of nearly one stone diameter. However, this causes some difficulties. Δx is generally not equal to the dimension of the stones. For instance, for small material, several stones are positioned within one Δx. For the number of stones within one Δx, $\Delta x/D$ can be taken. Δz can be determined in such a way that an area equal to the area of all stones within Δx is relocated. This solves the problem for the presence of more than one stone within one space-increment. A more detailed discussion concerning the numerical implementation is given in Van Gent (1993).

VERIFICATION OF RESPONSE MODEL

For the computations that were used for calibration and verification wave trains with 500 irregular waves have been used. The computations were done with a TMA spectrum (Texel, Marsen, and Arsloe data sets). This is a spectrum based on the JONSWAP spectrum but corrected for a finite water depth, (Bouws et al. 1985). Tests performed by Van der Meer (1988) were used for verification of the wave-response model. These physical model tests were performed with different spectra. However, neither Van der Meer (1988) nor Kao and Hall (1990) observed a clear influence of the spectral shape on the reshaping process. Therefore, these dissimilar spectra are assumed not to contribute to possible deviations between the measured and computed results. The spectra are represented by the significant wave height H_s and the mean wave period T_m. The material is characterized by the D_{n50}.

For the friction coefficients in the porous medium and for the added mass coefficient, the expressions given by Ven Gent (1994b) have been used. These expressions contain a characteristic velocity to take the influence of the wave climate into account; in the equation describing the flow through the permeable part, the friction term proportional to the squared velocity contains a coefficient that depends on the local flow field. This friction coefficient depends on the Keulegan-Carpenter number. In the case of irregular waves, the maximum velocity that occurred in the preceding time-inter-

val, with a length of one peak period, is taken for the characteristic velocity in the Keulegan-Carpenter number.

Before a verification of the model can be performed, several coefficients need to be assessed through calibration. These coefficients are the drag (c_D), lift (c_L), and inertia (c_M) coefficients as well as the coefficient for the influence of the pressure gradient (c_P). For calibration, one particular test is used where accretion occurs both above and below the still-water level in the dynamically stable situation. For this test, the measured profile and the empirical relations for the reshaped profile by Van der Meer (1988) hardly differ, and therefore these empirical relations are used for comparison with the numerical model results. The test concerns a uniform 1:3 slope and material with a diameter of 0.0110 m (D_{n50}). H_s, T_m, and the still-water level were 0.24 m, 1.8 s and 0.80 m, respectively. After several numerical model runs with different values of these calibration parameters, a suitable match was obtained with the following values: $c_D = 0.0175$, $c_L = 0.075$, $c_M = 0.08$, and $c_P = 0.01$. Fig. 10 shows the reshaped profile after 500 waves. For a second simulation with larger material, $D_{n50} = 0.0257$ m, the lifting process appeared to be underestimated. The lift coefficient c_L, for which 0.075 was taken, is apparently larger for larger material. For material larger than $D_{n50} = 0.0110$ m, a linear relation is used as a first approximation: $c_L = 7.85 \cdot D_{n50}$. The minimum and maximum values for c_L are set at 0.01 and 0.38. It must still be verified whether this relation must be improved. It appeared that the results are relatively sensitive to the values of c_D and c_L, whereas the results are not sensitive to the values of c_M and c_P. The values for c_D, c_M, and c_P and the relation for c_L are used for all following computations.

As mentioned before, the coefficients may be different for the initiation of movement (stones positioned in the cover layer are nonmoving stones [c_D, c_M]) than those for the movement along the slope (stones moving along the slope are moving stones [c_D, c_M]). For instance, the projected area is much smaller for a stone in the cover layer because it is partially sheltered by other stones. This is not the case for the stones that move along the slope. Because no sheltering has been taken into account, the coefficients may be much larger for the stones in the cover layer than for a stone moving along the slope. However, the coefficients are assumed to be the same here. Moreover, because the flow pattern around a moving stone differs from the pattern around a stable stone, it is likely that the coefficients are not the same for nonmoving and moving stones. Assuming that the nonmoving stone (c_D, c_M) is different from the moving stone (c_D, c_M), the following discussion can be made.

It appeared that the resistance against the failure mechanisms sliding and lifting often have the same shape. A stone that is now regarded as unstable due to lifting can become unstable at the same moment of time due to sliding. This means that instead of the used combination of c_D, c_M and c_L, the same unstable stone can be achieved with a larger c_D (resistance against sliding lower). However, the direction in which the stones move is much more sensitive for a correct combination of c_D and c_M. This means that the model is not sensitive for the combination of nonmoving stone (c_D, c_M) but sensitive for the combination of moving stone (c_D, c_M). Nonmoving stone (c_D, c_M) may therefore be different in reality without necessarily leading to different results. This may partially explain why Tørum (1992) found a considerably larger value for c_D—0.35 for a stable stone (nonmoving stone c_D)—instead of the value 0.0175 that is used here (moving stone c_D). Tørum (1992) found a value of 0.15 for c_M. Because the numerical model is not sensitive for the value of c_M, computations with $c_M = 0.15$ instead of the value 0.08 that has been used would not lead to very different results.

Twenty computations, representing the reshaping process of gravel beaches and berm breakwaters, have been performed to verify the combined wave-response model. The tests performed by Van der Meer (1988) have been used to derive expressions for the prediction of the reshaped profile. Conditions that these expressions have been derived from are used for comparison. Since for these tests the differences between the measured profiles and the profile derived from the expressions are relatively small, the expressions have been used for convenience. The seward slopes had uniform initial slopes of 1:5, 1:3, or 1:1.5 with stones of $D_{n50} = 0.0041$ m, $D_{n50} = 0.0062$ m, $D_{n50} = 0.0110$ m, and $D_{n50} = 0.0257$ m. Wave heights varied roughly between 0.14 m and 0.24 m (H_s), wave periods between 1.3 s and 2.5 s (T_m). The still-water level was 0.80 m in all tests. For the coefficients k_1, k_2, and μ, the values 0.66, 0.9, and 50° have been used [see (1)–(3), (5), and (6)]. Dynamically stable profiles can be classified using the parameter $H_s/\Delta D_{n50}$. For dynamically stable profiles, this value varies roughly between 3 and 500. This parameter varies roughly between 4 and 6 for berm breakwaters. This value is higher for gravel beaches. For the computations performed here, the parameter $H_s/\Delta D_{n50}$ varied between 4.2 and 35.5.

As expected, differences occurred between the measured and calculated profiles. Fig. 11 shows a comparison for a test with a slope 1:5 and stones with a size of 0.0062 m (D_{n50}). The wave height and wave period were 0.24 m (H_s) and 1.8 s (T_m), respectively. The parameter $H_s/\Delta D_{n50}$ was 23.5. Both

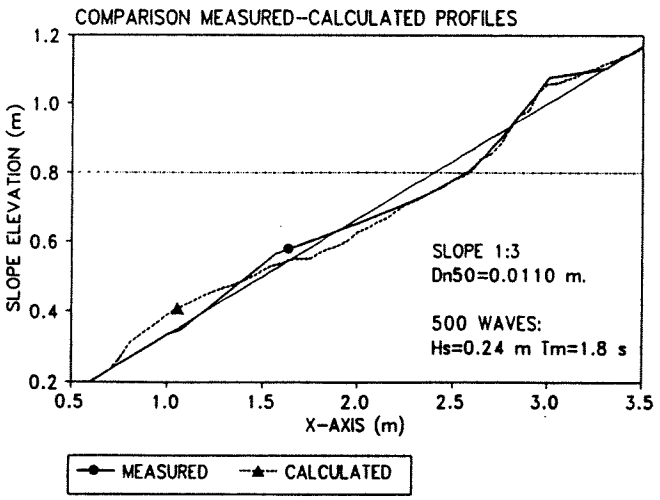

FIG. 10. Comparison between Measured and Calculated Profiles (Slope 1:3)

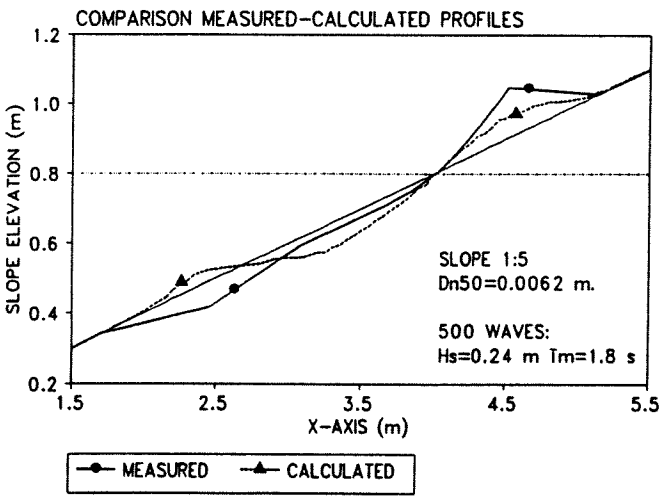

FIG. 11. Comparison between Measured and Calculated Profiles (Slope 1:5)

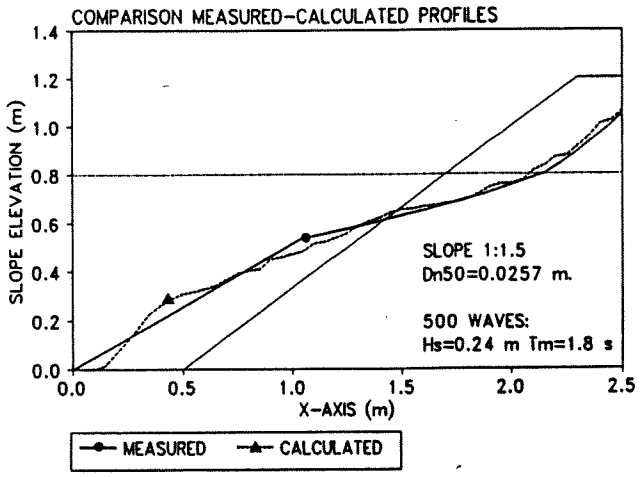

FIG. 12. Comparison between Measured and Calculated Profiles (Slope 1:1.5)

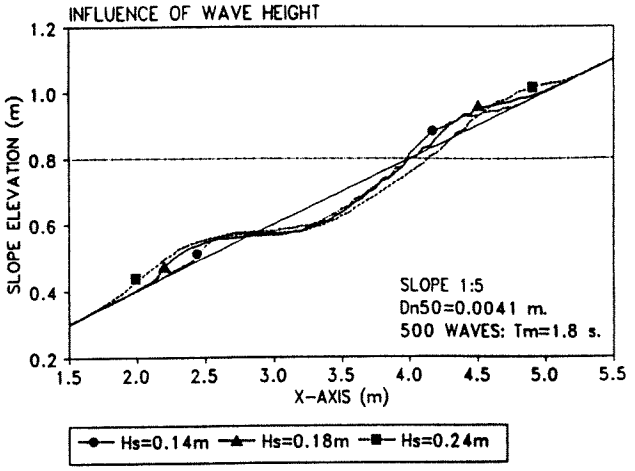

FIG. 13. Influence of Wave Height on Calculated Profiles

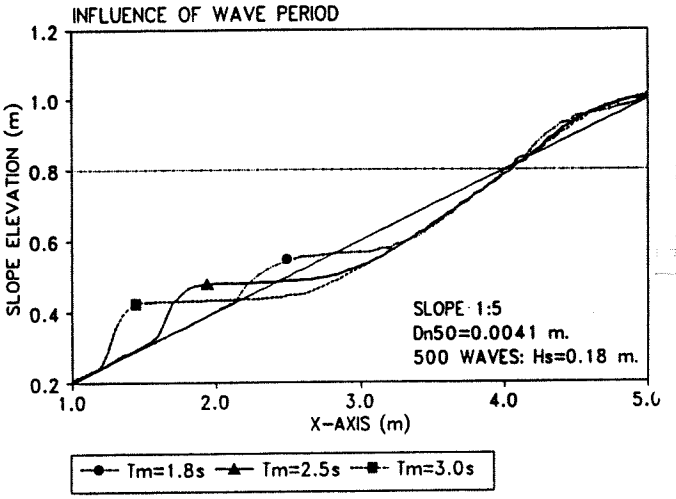

FIG. 14. Influence of Wave Period on Calculated Profiles

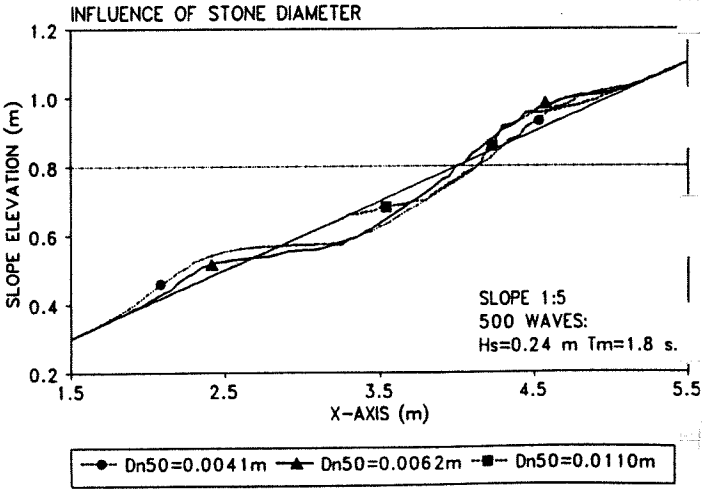

FIG. 15. Influence of Stone Diameter on Calculated Profiles

the physical model and the numerical model show accretion above the still-water level and erosion below the still-water level. However, the numerical model underestimates the accretion above the still-water level and the position of the area with erosion is located too far upward. Fig. 12 shows a comparison for a test with a slope 1:1.5 with stones with a size of 0.0257 m (D_{n50}). The irregular waves had a H_s = 0.24 m and T_m = 1.8 s. The parameter $H_s/\Delta D_{n50}$ was 5.7. The comparison between measured and calculated reshaped seaward profiles is good.

The results of the other comparisons can be found in Van Gent (1993). In most cases, the trends in the physical model tests and the numerical model results were the same; in most cases accretion and erosion took place in roughly the same sections as observed in the measurements. For the computations with 1:5 slopes, often both the accretion and the erosion were underestimated; for the computations with the 1:3 slopes, the comparison for the section above still-water level was good but the accretion below the still-water level was positioned too far downward; the computations with the 1:1.5 slopes showed a good comparison both above and below the still-water level. In general, it seemed as if accretion was underestimated in cases where it occurred above the still-water level, whereas it was overestimated where accretion occurred further down the slope. This conclusion, however, does not hold for all simulations.

For the calculation of forces, the model uses depth-averaged velocities rather than velocities near the bottom (slope). During up-rush, it is expected that a depth-averaged velocity is a rather good characteristic velocity in the runup area. More downward along the slope, the water depth increases. In this area, the depth-averaged velocity may differ much more from the velocity near the bottom. This partially explains the relatively weaker correspondence with the measurements for the section below the still-water level.

A qualitative verification has been performed to verify whether the influence of the variation of several parameters corresponds to those observed in physical-model tests. The parameters wave height, wave period, stone diameter, and the initial slope have been varied while the other parameters were kept constant. For each parameter variation, one example is shown in Figs. 13–16. It is clearly shown that an increased wave height or an increased wave period leads to longer reshaped profiles. This was also observed in physical model tests. Fig. 15 shows that smaller material results in a more affected slope. The simulations show that smaller material leads to more accretion below the still water level. This is not the case for the area above the still-water level. Fig. 16 shows three reshaped profiles with initial slopes of 1:1.5, 1:3, and 1:5. The figures shows that the reshaped profiles near the still-water line are hardly influenced by the initia slope. This also was observed in physical-model tests. Furthe upward or downward, the reshaped profiles evolve more toward the initial slope. It is concluded that the influence of the wave height, wave period, stone diameter, and initia slope are represented correctly.

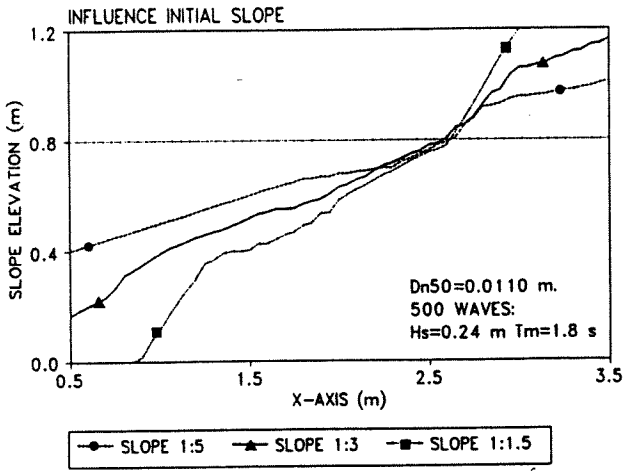

FIG. 16. Influence of Initial Slope on Calculated Profiles

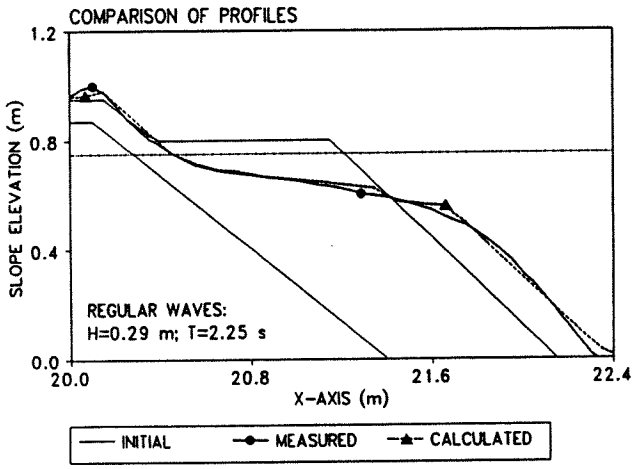

FIG. 17. Comparison between Measured and Simulated Profiles (Small-Scale Test)

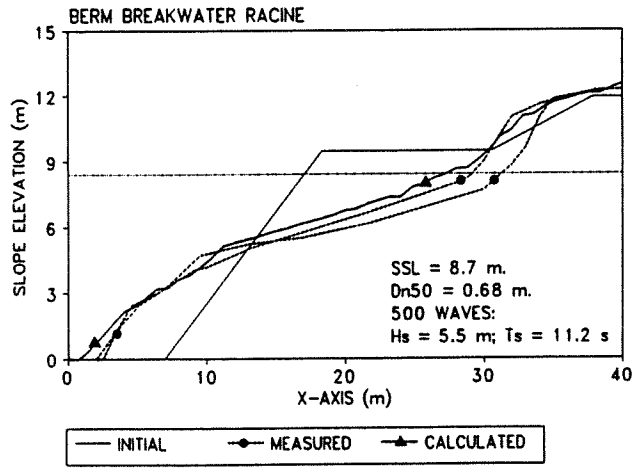

FIG. 18. Comparison between Measured and Simulated Profiles (Prototype)

SIMULATIONS WITH BERM BREAKWATERS

Now, some computations with initial slopes with a horizontal berm will be described. First, the reshaping process with the berm breakwater from the physical-model tests as shown in Fig. 4 is simulated. Regular waves were generated, unlike in all other computations. In the physical-model tests, the final reshaped profile was formed after four series of regular waves, the last of which formed the final reshaped profile. In the computation, the last wave series has been used; H = 0.29 m and T = 2.25 s. The numerical model cannot deal with two porous materials. Here, the berm breakwater was modeled as homogeneous since the permeability of the core material was rather close to the permeability of the cover material. The increase in crest height as observed in the measurements is underestimated (see Fig. 17). However, the comparison is good.

A computation with the prototype berm breakwater in Racine, Wis., has been performed. Montgomery et al. (1988) presented two measured reshaped profiles after a storm characterized by H_s = 5.5 m; T_s = 11.2 s, and a storm surge level (SSL) of 8.7 m. These parameters were determined with a hindcast method using observed storm wind data. The structure was made of stones with a D_{n50} of 0.68 m. It was modeled as homogeneous. For the porous friction coefficients, including added mass, the expressions by Van Gent (1994b) were used. Fig. 18 shows fair agreement between the two measured profiles and the calculated profile.

CONCLUSIONS

The numerical wave model has been verified with measured surface elevations and with measured runup and rundown levels. The comparison with results from the physical-model tests showed that the numerical model gives a rather good impression of the wave motion. Verifications with other hydraulic properties and other data sets indicated the same. Although breaking waves evolve somewhat quicker in the numerical model due to the approximation of nonlinear shallow-water equations, the model is suitable to be extended with a morphological model for cross-structure transport. Such a response model has been developed and implemented in the hydraulic model, which resulted in an interactive wave-response model. The new response model can also be used in combination with other wave models simulating individual waves. The combined model shows good agreement with measured reshaped profiles from gravel beaches and berm breakwater. Also, the influence of the parameters wave height, wave period, stone diameter, and initial slope are represented correctly. Although the combined model can still be improved, the model can already be used as an additional tool for the prediction of dynamically stable profiles.

ACKNOWLEDGMENTS

The financial support by the Commission of the European Communities by way of the Marine Science and Technology Program G6–Coastal Structures Project (contract 0032-C) and by Rijkswaterstaat (Dutch Governmental Water Control and Public Works Department) is gratefully acknowledged. J. W. van der Meer from Delft Hydraulics is acknowledged for his valuable comments on the analysis of the physical model tests and the numerical model results.

APPENDIX I. REFERENCES

Bouws, E., Günther, H., Rosenthal, W., and Vincent, C. L. (1985). "Similarity of the wind wave spectrum in finite depth water, I spectral form." *J. Geophys. Res.*, 90(C1), 975–986.

Den Beeker, R. C., and Vries, M. (1985). "Stability of top-layer elements; Research concerning failure mechanisms and damage-causing forces for breakwaters under monochromatic wave attack," MSc Thesis, Delft University of Technology, Delft, The Netherlands (in Dutch).

Hibberd, S., and Peregrine, D. H. (1979). "Surf and runup on a beach: A uniform bore." *J. Fluid Mech.*, 95(2), 323–345.

Hudson, R. Y. (1958). "Wave forces on breakwaters." *Trans.*, ASCE, 11B, 653.

Iribarren Cavanilles, R. (1938). *A formula for the calculation of rock fill dikes*. Revista de Obras Publicas, Panjas, Spain.

Kao, J. S., and Hall, K. R. (1990). "Trends in stability of dynamically

stable breakwaters." *Proc. Int. Conf. on Coast. Engrg. 1990*, ASCE, New York, N.Y., 2, 1730–1741.
Kobayashi, N., and Otta, A. K. (1987). "Hydraulic stability analysis of armour units." *J. Waterways, Port, Coast, and Oc. Engrg.*, ASCE, 113(2), 171–185.
Kobayashi, N., Otta, A. K., and Roy I. (1987). "Wave reflection and runup on rough slopes." *J. Waterways, Port, Coast, and Oc. Engrg.*, ASCE, 113(3), 282–298.
Montgomery, R. J., Hofmeister, G. J., and Baird, W. F. (1988). "Implementation and performance of berm breakwater design at Racine, WI." *Berm breakwaters; unconventional rubble mound breakwaters*, Nat. Res. Council of Canada, Ontario, Sep., 230–249.
Morison, J. R., O'Brien, M. P., Johnsen, J. W., and Schaff, S. A. (1950). "The forces exerted by surface waves on piles." *Petrol. Trans.*, American Institute of Mining Engrs., 189, 149–154.
Norton, P. A., and Holmes, P. (1992). "Armour displacement on reshaping breakwaters." *Proc. Int. Conf. on Coast. Engrg. 1992*, ASCE, New York, N.Y., 2, 1448–1460.
Sandstrøm, Å. (1974). "Wave forces on blocks of rubble mount breakwaters." *Bulletin No. 83*, Dept. of Civ. Engrg., Royal Inst. of Technol., Stockholm, Sweden.
Sigurdsson, G. (1962). "Wave forces on breakwater cap-stones." *J. Waterways and Harbour Div.*, ASCE, 88, 27–60.
Tørum, A. (1992). "Wave induced water particle velocities and forces on an armour unit on a berm breakwater." *MAST-G6S Report/ Report STF60-A91204*, Norwegian Hydrotech. Lab., Trondheim, Norway.
Van der Meer, J. W. (1988). "Rock slopes and gravel beaches under wave attack," PhD thesis, Delft University of Technology, Delft, The Netherlands.
Van Gent, M. R. A. (1993). *Berm breakwaters*. Delft Univ. of Technol., Delft, The Netherlands.
Van Gent, M. R. A. (1994a). "The modelling of wave action on and in coastal structures." *Coast. Engrg.*, Amsterdam, The Netherlands, 22(3–4), 311–339.
Van Gent, M. R. A. (1994b). "Permeability measurements for the modelling of wave action on and in porous structures." *Proc. Coastal Dynamics '94*, ASCE, New York, N.Y.
Van Gent, M. R. A., Tönjes, P., Petit, H. A. H., and van den Bosch, P. (1995). "Wave action on and in permeable structures." *Proc. Int. Conf. on Coast. Engrg. 1994*, ASCE, New York, N.Y.

APPENDIX II. NOTATION

The following symbols are used in this paper:

c_D = drag coefficient;
c_L = lift coefficient;
c_M = inertia coefficient;
c_P = pressure coefficient;
D = stone size;
D_{EQ} = equivalent sphere diameter defined as $D_{EQ} = (6M_{50}/\pi\rho_a)^{1/3}$;
D_{n50} = diameter (based on weight) of stone sample, exceede by 50% of material;
F_D = drag force;
F_I = inertia force;
F_L = lift force;
F_P = force caused by pressure gradient;
f = friction coefficient for external wave motion;
g = gravitational acceleration;
H = wave height;
H_s = significant wave height;
h = water depth;
k_1 = volume shape factor;
k_2 = area shape factor;
M_{50} = average mass of rock grading; determined by 50% value on mass distribution curve;
n = porosity;
T = oscillation/wave period;
T_m = mean wave period;
T_p = peak period
u = depth-averaged horizontal velocity;
W_s = submerged weight of stone;
x = coordinate in horizontal direction;
z = coordinate in vertical direction;
Δ = $\rho_s/\rho_w - 1$;
η = free-surface elevation;
μ = angle of internal friction;
υ = kinematic viscosity;
ξ = surf similarity parameter;
ρ_s = density of stone material;
ρ_w = density of water; and
ϕ = local slope angle.